13 Surface energy fluxes

13.1 Chapter summary

The overall energy balance at Earth's land surface requires that the energy gained from net radiation be balanced by the fluxes of sensible and latent heat to the atmosphere and the storage of heat in soil. These surface energy fluxes are an important component of Earth's global mean energy budget and are a primary determinant of surface climate. The annual energy balance at the land surface varies geographically in relation to incoming solar radiation and soil water availability. Over land, annual evaporation is highest in the tropics and generally decreases towards the poles. Geographic patterns of evaporation are explained in the context of Budyko's analysis of the control of evaporation by net radiation and precipitation. Energy fluxes vary over the course of a day and throughout the year, also in relation to soil water availability and the diurnal and annual cycles of solar radiation. The various terms in the energy budget (net radiation, sensible heat flux, latent heat flux, and soil heat flux) are illustrated for different climate zones and for various vegetation types over the course of a year and over a day. The Penman–Monteith equation illustrates relationships among net radiation, latent heat flux, sensible heat flux, and surface temperature. Soil experiments that alter surface albedo, surface resistance to evaporation, and thermal conductivity illustrate the importance of these surface properties in regulating surface temperature and energy fluxes.

13.2 Surface energy budget

Energy continually flows through the climate system. The Sun is the principal source of radiant energy, but all objects with a temperature greater than −273.15 °C (0 kelvin) emit longwave radiation in proportion to their temperature raised to the fourth power (equation 3.4). The solar and longwave radiation that impinges on the ground heats the surface. Some of the incoming solar radiation is reflected away from the surface. The surface also emits outgoing longwave radiation. The remaining radiation is the net radiation at the surface. Net radiation is dissipated in three ways.

Movement of air transports heat in a process known as convection (Chapter 3, section 3.3.3). A common example is the warmth felt as warm air rises from a radiator or the cooling of a breeze on a hot summer day. This heat exchange is called sensible heat. Greenhouse microclimates are an example of the warm temperatures that can arise in the absence of convective heat exchange (Avissar and Mahrer 1982; Mahrer *et al.* 1987; Oke 1987). It is generally thought that greenhouses provide a warm environment to grow plants because glass or other translucent coverings allow solar radiation to penetrate and warm the interior of the greenhouse while longwave radiation emitted by these warm interior surfaces is trapped within the greenhouse. This is the analogy that spawned the term "greenhouse effect" by which increasing concentrations of CO_2 in the atmosphere warm Earth's climate. While this can happen, the daytime warmth in greenhouses is largely a result of negligible convective heat exchange with the outside environment. The sensible heat from the warm interior surfaces is trapped within the greenhouse, warming the interior air.

Evaporation is another way in which heat is dissipated at the surface. Considerable energy is required to change the phase of water from liquid at the surface to vapor in air. Evaporation, therefore, involves a transfer of mass and energy to the atmosphere. Transfer of mass is seen as wet clothes dry on a clothesline. Heat loss is why a person may feel cold on a hot summer day when wet but hot after being dried with a towel. When water changes from liquid to gas (vapor), energy is absorbed from the evaporating surface without a rise in temperature. This latent heat of vaporization varies with temperature, but is $2.454 \times 10^6\ \mathrm{J\,kg^{-1}}$ at 20 °C (Table 3.2). A typical summertime rate of evaporation is 5 mm of water per day, which with a density of $1000\ \mathrm{kg\,m^{-3}}$ is equivalent to 5 kg water per square meter

($5\,kg\,m^{-2}/1000\,kg\,m^{-3} = 0.005\,m$). At a temperature of 20 °C, a water loss of $5\,kg\,m^{-2}\,day^{-1}$ is equivalent to a heat loss:

$$5\frac{kg}{m^2\,day} \times \frac{1\ day}{86\,400\,s} \times 2\,454\,000\frac{J}{kg} = 142\frac{W}{m^2}$$

This heat is transferred from the evaporating surface to the air, where it is stored in water vapor as latent heat. It is released when water vapor condenses back to liquid.

Some heat is exchanged with the underlying soil through conduction (Chapter 3, section 3.3.2). Conduction is the transfer of heat along a temperature gradient from high temperature to low temperature but in contrast to convection due to direct contact rather than movement of air. The heat felt when touching a steaming mug of coffee is an example of conduction.

Remembering that the change in energy storage in a system is equal to the difference between energy input and energy output (equation 3.8), the overall energy balance of a volume of soil with surface area $\Delta x\,\Delta y\,m^2$ and depth Δz m is

$$\rho c(\Delta T/\Delta t)\,\Delta z = (S\downarrow - S\uparrow + L\downarrow - L\uparrow) - H - \lambda E = G \quad (13.1)$$

The left-hand side of this equation represents the change in storage, where ρc is heat capacity ($J\,m^{-3}\,°C^{-1}$) and $\Delta T/\Delta t$ is the change in temperature with time ($°C\,s^{-1}$). The right-hand side of the equation represents the energy gained from incoming solar radiation ($S\downarrow$) and longwave radiation ($L\downarrow$) minus energy losses from reflected solar radiation ($S\uparrow$), outgoing longwave radiation ($L\uparrow$), sensible heat (H) and latent heat (λE). Latent heat flux is the product of the evaporative water flux (E, $kg\,m^{-2}\,s^{-1}$) times the latent heat of vaporization (λ, $J\,kg^{-1}$). The difference among net radiation, sensible heat flux, and latent heat flux is the heat flux (G) that is stored in the soil by conduction. The term Δz appears on the left-hand side of (13.1) because energy is stored in the soil volume with dimensions $\Delta x\,\Delta y\,\Delta z\,m^3$ while surface fluxes are exchanged over a surface area $\Delta x\,\Delta y\,m^2$; the common term ($\Delta x\,\Delta y$) drops out.

More commonly, the surface energy balance is written:

$$R_n = (S\downarrow - S\uparrow) + (L\downarrow - L\uparrow) = H + \lambda E + G \quad (13.2)$$

Net radiation is the total solar and longwave radiation absorbed by the surface after accounting for reflection of solar radiation and emission of longwave radiation. The net radiation absorbed by the ground surface is balanced by energy lost or gained by sensible heat, latent heat, and change in heat storage.

Consider, for example, a volume of soil 50 cm thick, deep enough so that no heat is conducted out of the bottom of the soil column over the course of a day. Typical energy fluxes at midday for a moist soil are $R_n = 650\,W\,m^{-2}$, $H = 200\,W\,m^{-2}$, $\lambda E = 350\,W\,m^{-2}$, and $G = 100\,W\,m^{-2}$. With a heat capacity of $2.5 \times 10^6\,J\,m^{-3}\,°C^{-1}$, typical of moist soil, the soil warms at a rate:

$$\Delta T/\Delta t = G/(\rho c \Delta z) = 0.29\,°C \text{ per hour}$$

13.3 Energy balance of Earth's surface

Energy is exchanged between the atmosphere and Earth's surface. Solar radiation and atmospheric longwave radiation heat the surface and provide energy to drive weather and climate. Some of this energy is stored in the ground or oceans. Some of it is returned to the atmosphere, heating the air. The rest is used to evaporate water. These surface energy fluxes are an important component of Earth's global mean energy budget. At the global scale, Earth's energy budget shows the atmosphere has a deficit of energy while the surface has a surplus (Fig. 4.9). The atmosphere absorbs $67\,W\,m^{-2}$ of solar radiation and $350\,W\,m^{-2}$ of longwave radiation; it emits $195\,W\,m^{-2}$ of longwave radiation to space and $324\,W\,m^{-2}$ to the surface. The excess loss of radiation compared with absorption is $-102\,W\,m^{-2}$. Earth's surface, in contrast, gains $168\,W\,m^{-2}$ of solar radiation and $324\,W\,m^{-2}$ of longwave radiation from the atmosphere while emitting $390\,W\,m^{-2}$ of longwave radiation. This gives the surface a net surplus of $102\,W\,m^{-2}$. This surplus energy is returned to the atmosphere as sensible heat ($24\,W\,m^{-2}$) and latent heat ($78\,W\,m^{-2}$). These heat fluxes arise as winds carry heat (sensible heat) and moisture (latent heat) away from the surface.

Although small compared with other fluxes in Earth's energy budget, sensible heat and latent heat are important terms in the energy budget. The majority of the net radiation at the surface is used to evaporate water rather than heat the surface. This latent heat is transferred to the atmosphere, where it is released when water vapor condenses and changes back from vapor to liquid. Release of this heat provides energy that fuels storms and atmospheric circulation. Over land, sensible and latent heat fluxes are important determinants of boundary layer climates. These are the climates near the ground and represent local climates due to topography, vegetation, soils, landforms, and structures.

The distribution of sensible and latent heat fluxes varies greatly with atmospheric conditions and soil moisture, but some general patterns can be seen (Fig. 13.1). Annual net radiation is largest in the tropics and deceases polewards. Oceans have greater net radiation than land because they absorb more solar radiation. Most of the radiative heating

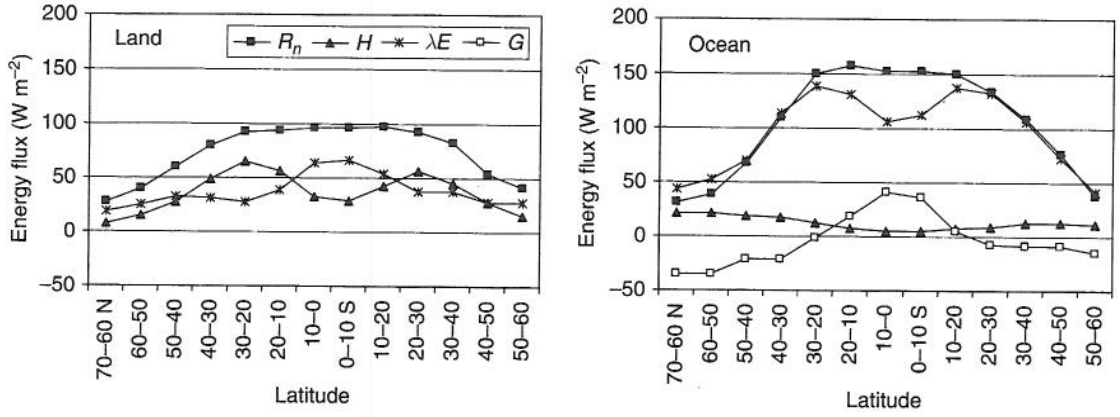

FIGURE 13.1. Annual average energy fluxes over land and ocean in relation to latitude. Data from Budyko (1974, p. 219). See also Sellers (1965, p. 103).

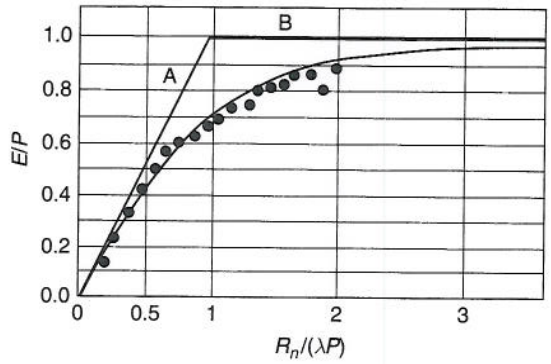

FIGURE 13.2. Relationship between the ratio of annual evaporation to precipitation (E/P) and the ratio of net radiation to the amount of energy required to evaporate the annual precipitation ($R_n/\lambda P$). Redrawn from Budyko (1974, p. 325).

of the oceans is balanced by evaporation. Ocean currents transport heat stored in tropical oceans to middle and high latitudes, where there is an annual loss of heat. Over land, annual evaporation is highest in the tropics and generally decreases towards the poles. Annual evaporation is a balance between radiative heating, which provides energy to evaporate water, and precipitation, which provides water to evaporate. In the tropics, there are large amounts of net radiation to evaporate water and there is ample precipitation year-round to sustain evaporation. Evaporation decreases in the subtropics (latitudes 10–30°). Here, there is still sufficient energy to evaporate water, but low annual precipitation reduces the availability of water to be evaporated. Evaporation increases somewhat in latitudes 30–50°, where storms are frequent. Sensible heat flux is lowest in the tropics, where annual evaporation is large, and increases in the subtropics, where arid conditions limit evaporation. At an annual timescale, heat storage in soil is negligible.

Typical values of the Bowen ratio (defined as the ratio of sensible heat flux to latent heat flux, $H/\lambda E$) are: 0.1–0.3 for tropical rainforests, where high annual rainfall keeps soil wet year-round; 0.4–0.8 for temperate forests and grasslands, where less rainfall causes drier soils; 2.0–6.0 for semi-arid regions with extremely dry soils; and greater than 10.0 for deserts (Oke 1987, p. 70).

Budyko (1974, pp. 322–327, 1986, pp. 76–79) proposed a relationship to describe geographic variation in annual evaporation (E) in term of annual precipitation (P) and annual net radiation (R_n). A key index is the ratio of net radiation to the amount of energy required to evaporate the annual precipitation. This latter term is given by λP, and the ratio $R_n/\lambda P$ is known as the radiative dryness index. Where the soil is dry, Budyko assumed that runoff is zero and all the precipitation evaporates provided there is sufficient net radiation to evaporate the water:

$$E \to P \text{ for } R_n \gg \lambda P, \text{ or, } \frac{E}{P} \to 1 \text{ as } \frac{R_n}{\lambda P} \to \infty \qquad (13.3)$$

This is represented by line B in Fig. 13.2. Where soil water is plentiful, evaporation is limited not by precipitation but rather by net radiation:

$$E \to \frac{R_n}{\lambda} \text{ for } R_n \ll \lambda P, \text{or, } \lambda E \to R_n \text{ as } \frac{R_n}{\lambda P} \to 0 \qquad (13.4)$$

This is represented by line A in Fig. 13.2. These two lines set the bounds on evaporation. Observations show, in fact, a smooth transition between these two limiting cases. The fitted relationship is

$$E = \left[\frac{R_n P}{\lambda}\left(\tanh\frac{\lambda P}{R_n}\right)\left(1 - \cosh\frac{R_n}{\lambda P} + \sinh\frac{R_n}{\lambda P}\right)\right]^{1/2} \qquad (13.5)$$

With $R = P - E$, (13.5) can be used to derive runoff. Figure 13.3 illustrates these relationships over a range of annual precipitation and net radiation. Analyses of climate model data show the generality of this relationship (Koster *et al.* 1999).

13.4 Annual cycle

The energy balance at the land surface varies seasonally due to changes in incoming solar radiation and precipitation. Figure 13.4 illustrates general trends in monthly surface fluxes for six climate zones. These are the fluxes to be expected based on prevailing climatology. The actual energy fluxes in a particular locale vary depending on vegetation, soil moisture, and meteorological conditions. However, some general geographic patterns are evident.

In the tropics, net radiation is high and relatively constant throughout the year. Much of this energy is used to evaporate water, but the annual cycle of evaporation varies depending on water availability. At São Gabriel in the Amazon region of Brazil, the climate is tropical rainforest. High amounts of rainfall keep the soil wet throughout the year. Most of the net radiation is dissipated as latent heat, which closely tracks net radiation throughout the year. Where there is a pronounced dry season, such as Ho Chi Minh City, latent heat flux and sensible heat flux have pronounced annual cycles. Latent heat flux is high during the rainy season when the soil is wet. It decreases markedly during the dry season, when most of the net radiation is dissipated as sensible heat.

Arid climates also have high net radiation because the clear skies allow much of the solar radiation at the top of the atmosphere to reach the ground. Consequently, the annual cycle of net radiation closely follows that of solar radiation. With little rainfall, evaporation is negligible, and most of the energy is sensible heat. A typical annual cycle is shown in Fig. 13.4 for Aswan, Egypt.

Net radiation has a pronounced annual cycle in middle and high latitudes. Climates with cold seasons (e.g., Barnaul and Turukhansk, Russia, Fig. 13.4) typically have a negative radiation balance in winter when snow covers the ground. Thereafter, radiation increases to a summer maximum before decreasing again in autumn. In these climates, latent heat flux is low during the cold season when there is little energy available to evaporate water and increases markedly in summer. Humid subtropical climates can have high rates of evaporation. For example, large amounts of summer rainfall at Miyazaki, Japan (Fig. 13.4) provide for large latent heat flux, which closely follows the annual cycle of net radiation. Elsewhere, where moisture availability limits evaporation, sensible heat flux is a large component of the energy balance.

The concepts embodied in Budyko's analysis of net radiation and precipitation as limiting controls of evaporation can be extended to the monthly timescale. Monthly evaporation can be assumed to be limited by the lesser of net radiation (energy to evaporate water) or precipitation (water supply). This, indeed, is the case where there is little inter-seasonal storage of water in soil. The left-hand panel in Fig. 13.5 illustrates monthly evaporation when there is no inter-seasonal storage of water in soil. Evaporation is controlled by net radiation during the period November–May when precipitation is plentiful, but is limited by precipitation during the dry season of June–October. With storage, however, water gained when precipitation exceeds evaporation is used to supply evaporation in months when there is energy available to evaporate water but precipitation is low. As shown in the right-hand panel of Fig. 13.5, storage of soil water leads to deviation from the expected control of evaporation by net radiation or precipitation (Milly 1994).

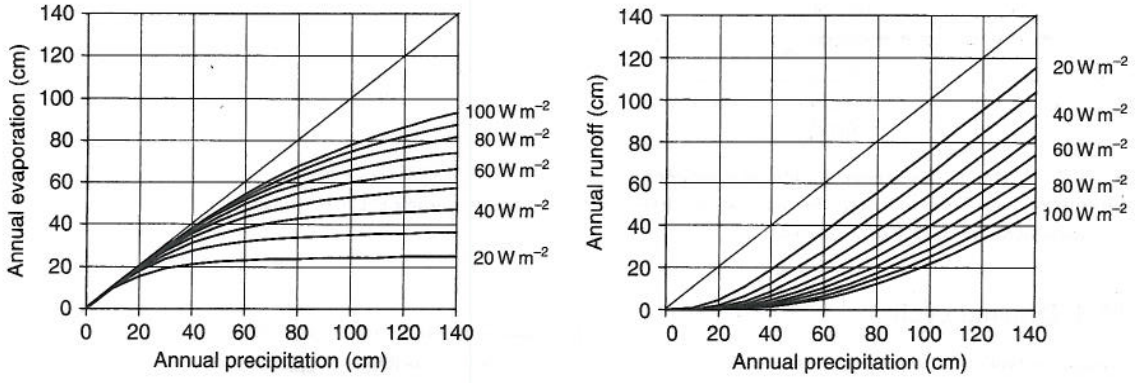

FIGURE 13.3. Relationships of annual evaporation (left) and annual runoff (right) with annual precipitation for annual net radiation ranging from 20–100 W m^{-2}. See also Budyko (1974, p. 327).

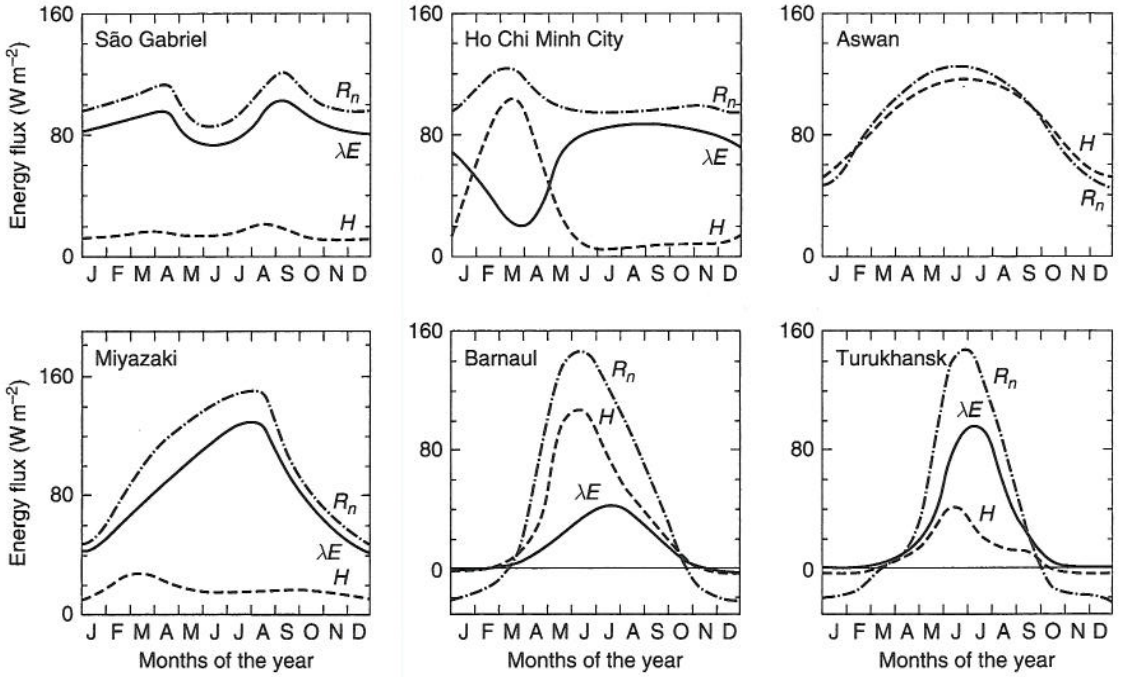

FIGURE 13.4. Monthly surface energy fluxes for six climate zones: São Gabriel, Brazil (0°08′ S, 67°05′ W), tropical rainforest; Ho Chi Minh City (10°47′ N, 106°42′ E), tropical savanna; Aswan, Egypt (24°02′ N, 32°53′ E), arid; Miyazaki, Japan (31°56′ N, 131°26′ E), humid subtropical; Barnaul, Russia (53°20′ N, 83°42′ E), humid continental cool summer; Turukhansk, Russia (65°47′ N, 87°57′ E), subarctic. Adapted from Budyko (1974, p. 193, p. 194, p. 195, p. 198, p. 200).

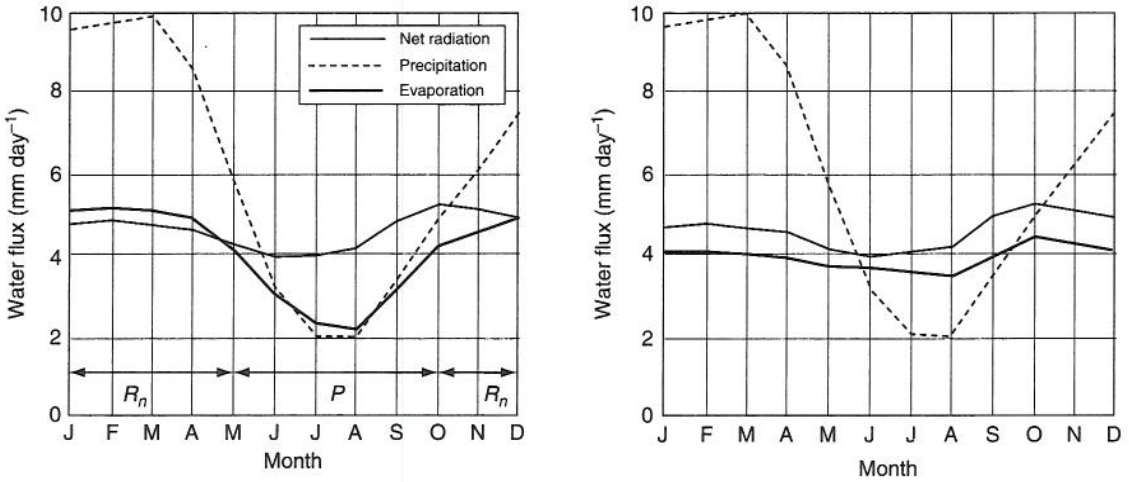

FIGURE 13.5. Monthly evaporation in relation to monthly precipitation and net radiation. Left: No inter-seasonal storage of soil water. Right: Inter-seasonal storage. From climate model simulations provided courtesy of David Lawrence (National Center for Atmospheric Research, Boulder, Colorado).

13.5 Diurnal cycle

Surface energy fluxes vary over the course of a day in response to the diurnal cycle of solar radiation. In early morning, the land surface typically has a negative radiative balance because no solar radiation is absorbed but long-wave radiation is lost. Sensible and latent heat fluxes are small. During daylight hours, the absorption of solar radiation increases and there is a net gain of radiation at the

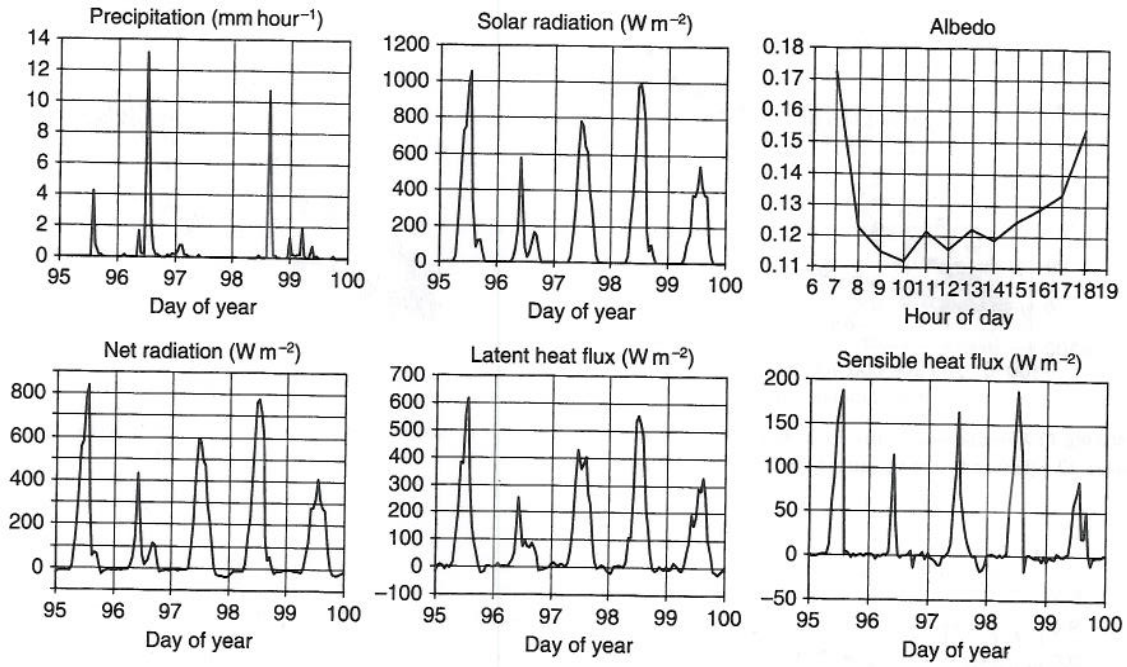

FIGURE 13.6. Hourly precipitation, incident solar radiation, net radiation, latent heat flux, and sensible heat flux for a tropical rainforest in southwestern Amazonia over a 5-day period (5–9 April 1993). Also shown is the average albedo for this period. Data are from the Anglo–Brazilian Amazonian Climate Observation Study (ABRACOS) for a forest near the town of Ji-Paraná in Rondônia (10°05′ S, 61°55′ W). The ABRACOS study is described by Gash *et al.* (1996) and the tower fluxes by Grace *et al.* (1995, 1996).

surface. The land warms and some of this energy is returned to the atmosphere as sensible and latent heat. The remainder warms the soil. Fluxes typically are strongest in early to middle afternoon and decrease late in the afternoon when solar radiation diminishes.

Figure 13.6 illustrates the diurnal cycle over a 5-day period for a tropical rainforest in Amazonia. In general, most of the net radiation during the measurement period was dissipated as latent heat. For this period, the Bowen ratio was 0.20, indicative of a wet site. The evaporative fraction (defined as the ratio of latent heat flux to the sum of sensible and latent heat fluxes, $\lambda E/[H+\lambda E]$) was 0.83. The occurrence of rain greatly affected surface fluxes. Cloudy and rainy conditions suppressed incoming solar radiation, net radiation, and latent heat flux on 6 and 9 April. In contrast, clear skies on 5 and 8 April allowed for large amounts of solar radiation (1000 W m^{-2}) and net radiation (>750 W m^{-2}) to heat the surface, with correspondingly high latent heat flux (>550 W m^{-2}). On these two days, afternoon rainstorms reduced latent heat flux from these high clear-sky values. For example, highest latent heat flux (618 W m^{-2}) occurred at 1300 local time on 5 April, when solar radiation was 1053 W m^{-2} and net radiation was 837 W m^{-2}. A rainstorm over the next hour reduced solar radiation (345 W m^{-2}) and net radiation (274 W m^{-2}), and latent heat decreased to 303 W m^{-2}. Overall, latent and sensible heat fluxes increased linearly with net radiation over this time period (Fig. 13.7).

Figure 13.8 illustrates the diurnal cycle for an aspen forest and two jack pine forests in Canada. On an average summer day (19 July–10 August 1994), latent heat exchange was an important means of dissipating the energy absorbed by the aspen forest. At midday, about one-half the net radiation absorbed by the forest was returned to the atmosphere as latent heat. This was over twice the sensible heat flux, indicating a well-watered site. In contrast, latent heat and sensible heat were comparable in magnitude earlier in the growing season (24 May–16 June 1994). The Bowen ratio decreased from 0.68 early in the growing season to 0.13 in summer as the evaporative fraction increased from 0.59 to 0.88. The jack pine forests had much less latent heat flux than the aspen forest. Midday fluxes were on the order of 100 W m^{-2} or less compared with 250 W m^{-2} for the aspen forest. In the jack pine forests, sensible heat was the dominant means to dissipate net radiation. The northern jack pine forest had less midday net radiation than the southern forest, resulting in lower sensible and latent heat fluxes. The dry environments of the jack pine forests are seen it their Bowen ratios of 1.45 (southern site) and 1.31 (northern site) and evaporative fractions of 0.41 and 0.43, respectively.

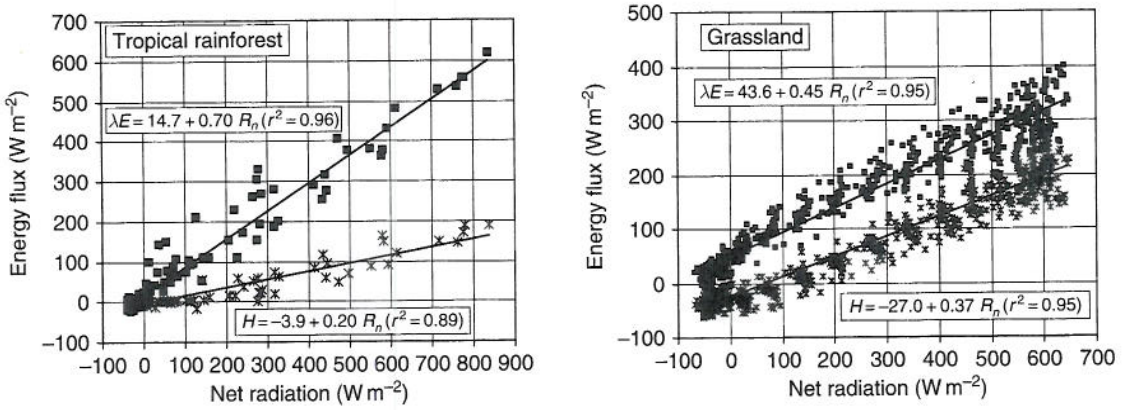

FIGURE 13.7. Relationship of latent heat flux (λE) and sensible heat flux (H) with net radiation (R_n) for the tropical rainforest shown in Fig. 13.6 (left) and for the grassland shown in Fig. 13.9 (right).

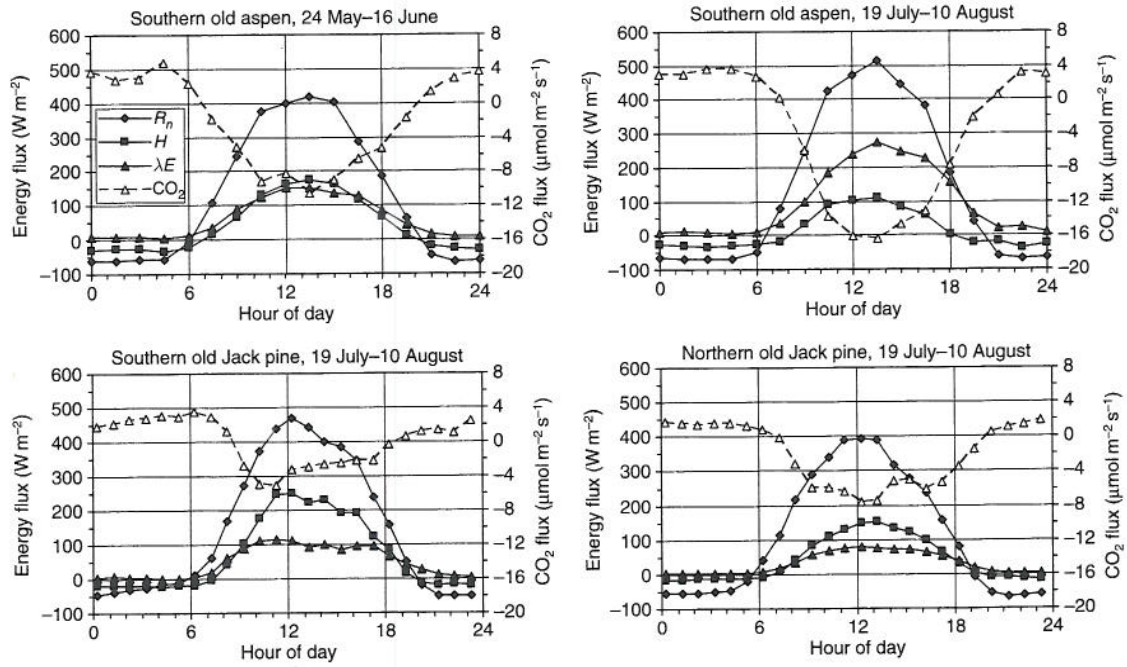

FIGURE 13.8. Diurnal cycle of net radiation (R_n), sensible heat (H), latent heat (λE), and CO_2 for three boreal forests in Canada. Data are from the Boreal Ecosystem Atmosphere Study (BOREAS) for an aspen (*Populus tremuloides*) forest in Prince Albert National Park, Saskatchewan, Canada (53°38′ N, 106°12′ W), a jack pine (*Pinus banksiana*) forest near Nipawin, Saskatchewan, Canada (53°55′ N, 104°41′ W), and a jack pine forest near Thompson, Manitoba (55°56′ N, 98°37′ W). The tower fluxes are described by Blanken *et al.* (1997), Baldocchi *et al.* (1997), and Moore *et al.* (2000), respectively. Data are averaged for the period 24 May–16 June 1994 and 19 July–10 August 1994 as described by Bonan *et al.* (1997).

Figure 13.9 illustrates surface energy fluxes over a 20-day period for grassland in Kansas. No rain fell from 19 July to 2 August 1987 (days 200–214). Latent heat flux was the dominant flux when soil was wet. As the soil dried, latent heat flux declined and sensible heat flux increased. Rainfall towards the end of the 20-day period wetted the soil and latent heat flux increased from the previous day. Soil heat flux was a significant portion of the energy budget throughout the period. For this period, the Bowen ratio was 0.31 and the evaporative fraction was 0.76. Latent and sensible heat fluxes increased linearly with net radiation (Fig. 13.7).

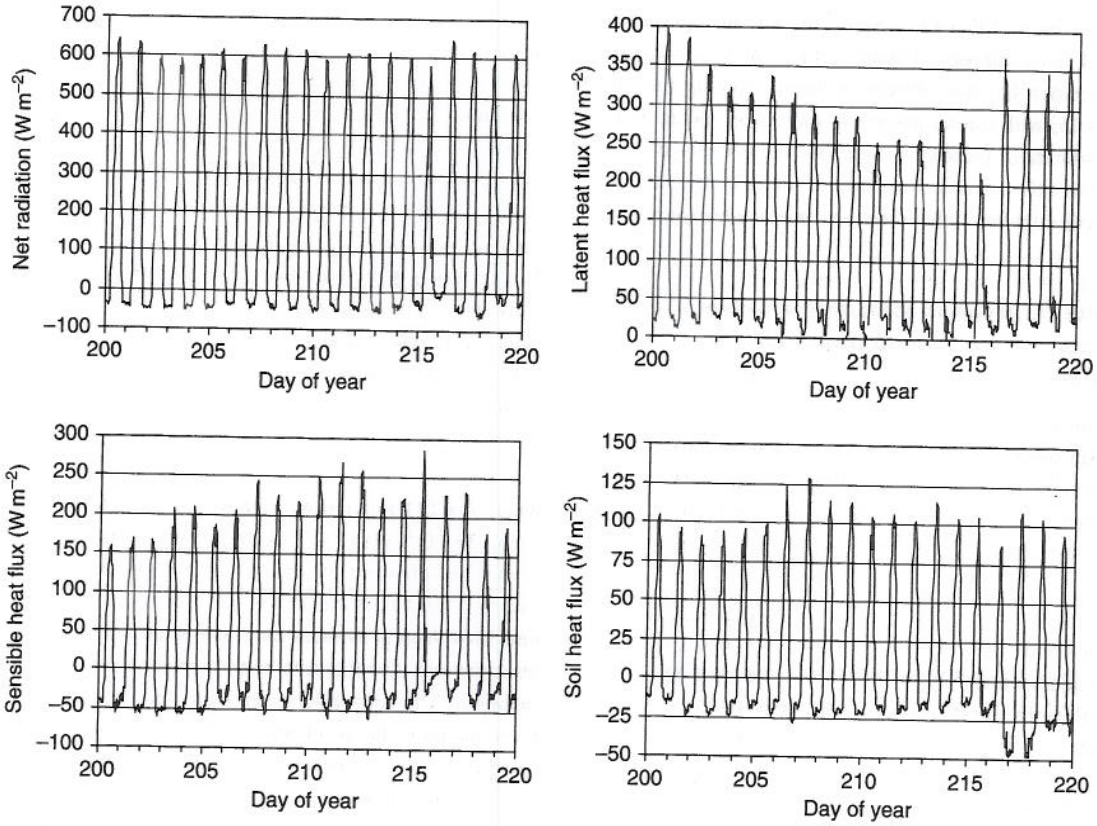

FIGURE 13.9. 30-minute fluxes of net radiation, latent heat, sensible heat, and soil heat for grassland during the 20-day period 19 July–7 August 1987. Data are from the First ISLSCP (International Satellite Land Surface Climatology Project) Field Experiment (FIFE) and averaged for the 15 km × 15 km study site near Manhattan, Kansas (39°03′ N, 96°32′ W) as described by Betts and Ball (1998).

Figure 13.10 illustrates surface energy fluxes for semi-arid vegetation in the Sonoran Desert near Tucson, Arizona. During dry periods, latent heat flux was small (about 50 W m^{-2}), and most of the net radiation was dissipated as sensible heat. Sensible heat flux peaked in the middle of the afternoon. Soil heat flux was a sizable portion of the surface energy balance and attained peak values before noon. The Bowen ratio averaged for this day was 6.92 and the evaporative fraction was 0.13, both indicative of dry soil. In late August, monsoonal rains wetted the soil and produced a different diurnal cycle. Sensible heat flux decreased substantially compared with the dry day and latent heat flux increased due to the wet soil. The lower Bowen ratio (0.63) and higher evaporative fraction (0.61) are indicative of the wetter soil.

13.6 Energy balance model

The effect of different surfaces on energy fluxes and surface climate can be understood using a simple one-dimensional model of the surface energy balance (Gates 1980; Grace 1983; Monteith and Unsworth 1990; Campbell and Norman 1998).

13.6.1 Net radiation

Not all of the solar radiation impinging on the ground surface is used to heat the surface. Some of the incident solar radiation is reflected; the remainder is absorbed. The amount reflected is

$$S\uparrow = rS\downarrow \tag{13.6}$$

where $S\downarrow$ is the incident radiation onto the surface and r is the albedo, defined as the fraction of $S\downarrow$ that is reflected by the surface. The remainder, $(1 - r)S\downarrow$, is the solar radiation absorbed by the surface. A perfect mirror has an albedo of one (i.e., all the incoming light is reflected). An object that completely absorbs all radiation incident upon its surface, known as a blackbody, has an albedo of zero (i.e., all light is absorbed).

Albedos typically range from about 0.80 to 0.95 for fresh snow to as little as 0.03–0.10 for water at low solar

zenith angle (Table 13.1). Snow, deserts, and glaciers have the highest albedos. Urban surfaces have low albedos. Vegetation has low albedos, typically ranging from 0.05 to 0.25, with forests absorbing more solar radiation than grasslands or croplands. Soil albedo generally decreases with coarser particle size. Coarse soil particles trap radiation through multiple reflections among adjacent particles. In contrast, fine soil particles expose a relatively uniform surface, trapping less radiation. Soil albedo also decreases with soil wetness because radiation is trapped by internal reflection.

TABLE 13.1. Broadband albedo of various surfaces

Surface	Albedo
Natural	
Fresh snow	0.80–0.95
Old snow	0.45–0.70
Desert	0.20–0.45
Glacier	0.20–0.40
Soil	0.05–0.40
Cropland	0.18–0.25
Grassland	0.16–0.26
Deciduous forest	0.15–0.20
Coniferous forest	0.05–0.15
Water	0.03–0.10
Urban	
Road	0.05–0.20
Roof	0.08–0.35
Wall	0.10–0.40
Paint	
White	0.50–0.90
Red, brown, green	0.20–0.35
Black	0.02–0.15

Source. Data from Oke (1987, p. 12, p. 281).

Similarly, not all the longwave radiation incident on the ground surface is used to heat the surface. Terrestrial objects emit electromagnetic radiation in the infrared band at long wavelengths between 3 μm and 100 μm. This emission is proportional to temperature raised to the fourth power. In addition, some of the incoming longwave radiation is reflected by the surface. For temperature in degrees Celsius the outgoing longwave radiation from the surface is

$$L\uparrow = \varepsilon\sigma(T_s + 273.15)^4 + (1-\varepsilon)\mathrm{L}\downarrow \qquad (13.7)$$

where $T_s + 273.15$ is absolute temperature in kelvin (K) and $\sigma = 5.67 \times 10^{-8}$ W m^{-2} K^{-4} is the Stefan–Boltzmann constant. The emissivity (ε) of land surfaces generally ranges from 0.90 to 1.0. A blackbody has an emissivity equal to one. Most natural surfaces are gray bodies with emissivity less than one. The first term in this equation is the emitted radiation. The second term represents the incident longwave radiation that is reflected to space. The emissivity of a surface is also its absorptivity so that $(1-\varepsilon)$ is the fraction of incoming longwave radiation $L\downarrow$ that is reflected.

13.6.2 Sensible heat flux

Sensible heat flux can be represented through a resistance network in which heat flux is directly proportional to the temperature difference between the surface and the surrounding air and inversely proportional to a transfer resistance:

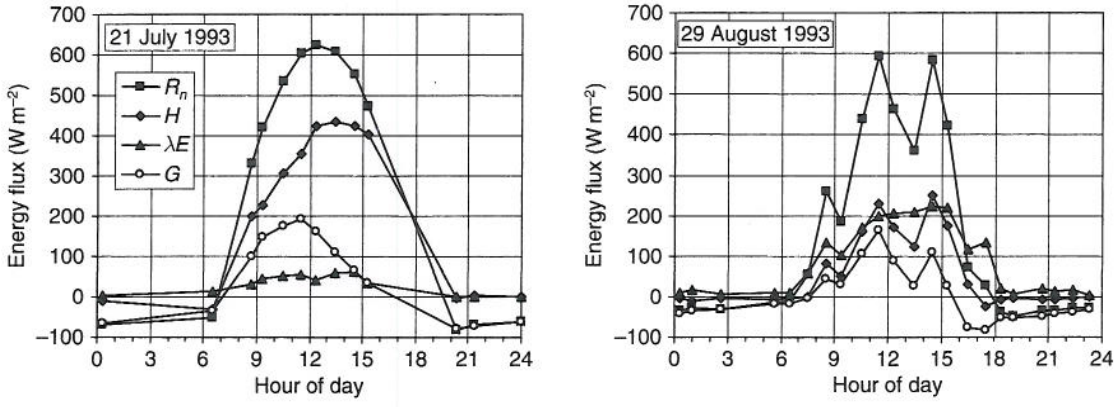

FIGURE 13.10. Diurnal cycle of net radiation (R_n), sensible heat (H), latent heat (λE), and soil heat (G) for semi-arid Sonoran desert near Tucson, Arizona (32°13′ N, 111°05′ W) on a typical dry day with clear sky (left) and with wet soil during monsoonal rains (right). Data from Unland *et al.* (1996).

$$H = -\rho C_p \frac{(T_a - T_s)}{r_H} \tag{13.8}$$

where T_s and T_a are the surface and air temperatures (°C), respectively. An object loses energy if its temperature is warmer than the air (a positive flux); it gains energy when it is colder than the air (a negative flux). The density of air (ρ, kg m^{-3}) varies with temperature and humidity but $\rho = 1.15$ kg m^{-3} is typical. The term C_p is the heat capacity of air and is approximately 1005 J kg^{-1} °C^{-1}. The resistance r_H (s m^{-1}) depends on wind speed and surface characteristics. A typical value is on the order of 20–100 s m^{-1}. For example, a surface that is 5 °C warmer than the air has a sensible heat flux of 289 W m^{-2} with $r_H = 20$ s m^{-1}.

For ground and vegetated surfaces, the resistance depends in part on surface roughness (Chapter 14). Sensible heat is exchanged between land and atmosphere because of turbulent mixing of air and resultant transport of heat, generally away from the surface during the day. Turbulence occurs when wind flows over Earth's surface and the ground, trees, grasses, and other objects retard the fluid motion of air. Taller objects are rougher than shorter objects, exert more drag on air flow, and generate more turbulence, all other factors being equal. Surface roughness varies greatly with the type of surface (Table 14.1).

13.6.3 Latent heat flux

Latent heat flux is represented by a resistance network similar to sensible heat:

$$\lambda E = -\frac{\rho C_p}{\gamma} \frac{(e_a - e_*[T_s])}{r_W} \tag{13.9}$$

The term $e_*[T_s]$ represents the saturation vapor pressure (Pa) evaluated at the surface temperature, and e_a is the vapor pressure of air (Pa). The term γ is the psychrometric constant, which depends on heat capacity (C_p, J kg^{-1} °C^{-1}), atmospheric pressure (P, Pa), and latent heat of vaporization (λ, J kg^{-1}) as $\gamma = (C_p P)/(0.622\lambda)$ A typical value is 66.5 Pa °C^{-1}. The term r_W is a resistance (s m^{-1}) analogous to r_H. This resistance depends on meteorological conditions similar to r_H, but also increases as the surface becomes drier (i.e., less saturated) so that a wet site has a higher latent heat flux than a dry site, all other factors being equal. This equation is analogous to that for sensible heat flux, and a positive flux means loss of heat and water to the atmosphere.

The term $e_*[T_s] - e_a$ is the vapor pressure deficit between the evaporating surface, which is saturated with moisture, and air. Saturation vapor pressure increases exponentially with higher temperature (Fig. 3.3) so that evaporation increases with higher temperature, all other factors being equal. Consider, for example, a surface with a temperature of 25 °C. Its saturation vapor pressure is approximately 3167 Pa. If the surrounding air has a vapor pressure of 1584 Pa (50% relative humidity at 25 °C), the latent heat flux is 275 W m^{-2} with $r_W = 100$ s m^{-1}. Latent heat flux increases to 462 W m^{-2} when the same air is in contact with a surface with a temperature of 30 °C (saturation vapor pressure is approximately 4243 Pa).

Alternatively, (13.9) can be written:

$$E = -\rho(q_a - q_s)/r_W \tag{13.10}$$

where E is water vapor flux (kg m^{-2} s^{-1}) and q is specific humidity (kg kg^{-1}). Substitution of $q = 0.622e/P$ and multiplying by the latent heat of vaporization (to convert E with units kg m^{-2} s^{-1} to λE with units W m^{-2}) gives (13.9).

13.6.4 Soil heat flux

The rate at which heat is exchanged by conduction between the surface and the underlying soil depends on the temperature gradient and thermal conductivity (Chapter 9). For a surface with temperature T_s (°C), the heat transfer to or from soil with a temperature T_g (°C) at a depth Δz (m) is

$$G = k(T_s - T_g)/\Delta z \tag{13.11}$$

where k is thermal conductivity (W m^{-1} °C^{-1}). Thermal conductivity is a measure of an object's ability to conduct heat. Differences in thermal conductivity can create perceptions of hot or cold when touching an object. A metal spoon in a cup of hot soup feels warmer than a wooden spoon because it conducts heat from the soup to a person's hand much more rapidly than a wooden spoon. The rate of heat transfer by conduction increases with larger temperature gradient and with larger thermal conductivity.

13.6.5 Surface temperature

The net radiation that impinges on a surface or object must be balanced by energy lost or gained through sensible heat, latent heat, and conduction. This balance is maintained by the surface temperature. The energy balance at the ground surface is

$$(1 - r)S\downarrow + \varepsilon L\downarrow = \varepsilon\sigma(T_s + 273.15)^4 + H + \lambda E + G \tag{13.12}$$

The left-hand side of this equation constitutes the radiative forcing (Q_a), which is the sum of absorbed solar radiation and absorbed longwave radiation, respectively.

The right-hand side of the equation consists of the emitted longwave radiation, sensible heat flux, latent heat flux, and heat storage in soil by conduction. The surface temperature (T_s) is the temperature that balances this energy budget:

Latent heat flux increases as net available energy ($R_n - G$) increases and decreases as sensible heat flux (H) increases. For a constant value of $R_n - G$ latent heat flux decreases as surface temperature (T_s) increases (Fig. 13.11).

$$(1-r)S\downarrow + \varepsilon L\downarrow = \varepsilon\sigma(T_s + 273.15)^4 - \rho C_p \frac{(T_a - T_s)}{r_H} - \frac{\rho C_p}{\gamma}\frac{(e_a - e_*[T_s])}{r_W} + k\frac{(T_s - T_g)}{\Delta z} \tag{13.13}$$

This equation can be solved to obtain surface temperature. The expression for surface fluxes and temperature given by (13.13) is a non-linear equation that is difficult to solve without numerical methods. The Penman–Monteith equation provides a more simplified expression for sensible and latent heat fluxes and surface temperature.

13.7 Penman–Monteith equation

Penman (1948) combined the thermodynamic and aerodynamic aspects of evaporation into a mathematical equation that provides a simple means to study the surface energy budget and surface temperature (see review by Monteith 1981). The evaporation of water from a saturated surface is a thermodynamic process in which energy is required to change water from liquid to vapor. From (13.2) and (13.8), latent heat flux is

$$\lambda E = (R_n - G) - H = (R_n - G) + \rho C_p(T_a - T_s)/r_H \tag{13.14}$$

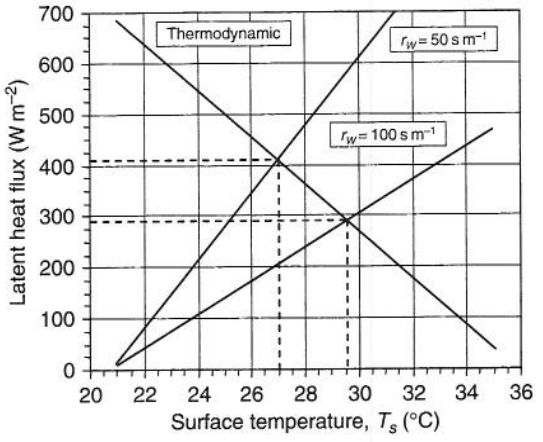

FIGURE 13.11. Thermodynamic (13.14) and aerodynamic (13.16) formulations of latent heat flux in relation to surface temperature. For this example, $R_n - G = 500$ W m^{-2}, $T_a = 25$ °C, relative humidity is 75%, and $r_H = 25$ s m^{-1}. The aerodynamic equation is shown for $r_W = 50$ s m^{-1} and $r_W = 100$ s m^{-1}. The thermodynamic and aerodynamic equations intersect at the appropriate surface temperature.

Evaporation is also an aerodynamic process related to the turbulent transport of water vapor away from the surface. This is represented by (13.9), in which latent heat flux increases as evaporative demand ($e_a - e_*[T_s]$) increases. The saturation vapor pressure at the surface temperature ($e_*[T_s]$), which is a non-linear function of temperature, can be approximated by

$$e_*[T_s] = e_*[T_a] + s(T_s - T_a) \tag{13.15}$$

where $e_*[T_a]$ is the saturation vapor pressure evaluated at the air temperature (T_a) and $s = de_*[T_a]/dT$ is the slope of the saturation vapor pressure versus temperature evaluated at T_a. Substituting (13.15) into (13.9) gives

$$\lambda E = \frac{\rho C_p}{\gamma}\frac{(e_*[T_a] + s(T_s - T_a) - e_a)}{r_W} \tag{13.16}$$

In (13.16), latent heat flux increases as surface temperature increases (Fig. 13.11).

Latent heat flux is obtained by finding the surface temperature that satisfies (13.14) and (13.16). From (13.14):

$$T_s - T_a = (r_H/\rho C_p)(R_n - G - \lambda E) \tag{13.17}$$

Substituting (13.17) into (13.16):

$$\lambda E = \frac{s(R_n - G) + \rho C_p(e_*[T_a] - e_a)/r_H}{s + \gamma(r_W/r_H)} \tag{13.18}$$

It is common to write $\gamma^* = \gamma\,(r_W/r_H)$ The original derivation by Penman (1948) was for evaporation over open water. Equation (13.18) has since been extended to a leaf (Chapter 16) or plant canopy (Chapter 18) by substituting the appropriate resistances and is commonly referred to as the Penman–Monteith equation (Monteith 1965). This equation shows that evaporation is a weighted linear combination of net available energy ($R_n - G$) and the vapor pressure deficit of air ($e_*[T_a] - e_a$).

The corresponding sensible heat flux is

$$H = \frac{(R_n - G)\gamma^* - \rho C_p(e_*[T_a] - e_a)/r_H}{s + \gamma^*} \tag{13.19}$$

and the surface temperature is

$$T_s = T_a + \frac{(R_n - G)\gamma^* r_H/\rho C_p - (e_*[T_a] - e_a)}{s + \gamma^*} \quad (13.20)$$

Figure 13.11 illustrates the solution of these equations. In this example, a resistance $r_W = 100\ \mathrm{s\ m^{-1}}$ gives $T_s = 29.6\ ^\circ\mathrm{C}$ and the net available energy is partitioned as $\lambda E = 288\ \mathrm{W\ m^{-2}}$ and $H = 212\ \mathrm{W\ m^{-2}}$. A smaller resistance ($r_W = 50\ \mathrm{s\ m^{-1}}$) yields greater latent heat flux ($407\ \mathrm{W\ m^{-2}}$), less sensible heat flux ($93\ \mathrm{W\ m^{-2}}$), and a cooler surface ($27.0\ ^\circ\mathrm{C}$). In general, surface temperature deceases as latent heat flux increases, all other factors being equal.

13.8 Soil microclimates

The use of paper, hay, and black plastic mulches to cover soil illustrates the effect of surface properties on energy fluxes and surface temperature (Table 13.2). These mulches alter surface albedo, surface resistance to evaporation, and thermal conductivity. At midday on the warm summer day when measurements were made, the uncovered soil had a surface temperature of 40 °C. Almost one-third of the net radiation was dissipated as latent heat. All mulches reduced evaporation compared with bare soil, but they differed in their effect on surface temperature. The soil covered with paper was similar in temperature to the bare soil. Although evaporation was reduced compared with the bare soil, much less radiation was absorbed at the surface due to the high albedo of the light-colored surface. In contrast, soil covered with black plastic had a temperature of 52 °C. This material was hot because of its low albedo and because the plastic barrier prevented evaporation. Instead, most of the net radiation was dissipated as sensible heat. The hay mulch also was hot (51 °C). In this case, the surface absorbed radiation similar to the bare soil. However, the mulch reduced evaporation and hindered heat transfer to the underlying soil due to low thermal conductivity.

Surface albedo can be purposely altered to change soil temperature. In one such study, a white powder was applied to cool soil temperature (Table 13.3). In the untreated soil, 30% of incoming solar radiation was reflected. Net radiation ($6.2\ \mathrm{MJ\ m^{-2}\ day^{-1}}$) was partitioned primarily as latent heat. Whitening the soil surface increased albedo so that 60% of incoming solar radiation was reflected. This reduced net radiation at the surface despite a reduction in outgoing longwave radiation brought about by the cooler surface. Less radiation was available to warm the soil or evaporate water. The soil cooled by 5 °C and evaporation decreased by 19%. Because the treated surface was colder than the air, sensible heat flux changed direction and was transferred to the colder surface.

TABLE 13.2. Midday summer energy balance ($\mathrm{W\ m^{-2}}$) and temperature (°C) for bare ground and soil covered with paper, hay, and black plastic mulch

		Mulch		
	Bare ground	Paper	Hay	Black plastic
Net radiation, R_n	642	433	607	712
Sensible heat, H	362	349	489	635
Latent heat, λE	195	42	84	0
Soil heat, G	85	42	35	77
Temperature, T_s	40	40	51	52

Source. Data from Rosenberg *et al.* (1983, p. 196).

TABLE 13.3. Surface energy budget ($\mathrm{MJ\ m^{-2}\ day^{-1}}$) and surface temperature (°C) for untreated and whitened soils

	Untreated soil	Whitened soil
Incoming solar radiation, $S\downarrow$	27.2	27.2
Reflected solar radiation, $S\uparrow$	8.2	16.3
Net longwave radiation, $L\downarrow - L\uparrow$	−12.8	−9.8
Net radiation, R_n	6.2	1.1
Sensible heat, H	1.9	−2.5
Latent heat, λE	4.2	3.4
Soil heat, G	0.2	0.2
Temperature, T_s	33 °C	28 °C

Source. Data from Stanhill (1965).

13.9 Review questions

1. A soil has energy fluxes $R_n = 450\ \mathrm{W\ m^{-2}}$, $H = 350\ \mathrm{W\ m^{-2}}$, and $\lambda E = 45\ \mathrm{W\ m^{-2}}$. Calculate the rate of warming. Another soil has energy fluxes $R_n = 600\ \mathrm{W\ m^{-2}}$, $H = 475\ \mathrm{W\ m^{-2}}$, and $\lambda E = 85\ \mathrm{W\ m^{-2}}$. Which soil warms faster? Assume $\rho c = 2.5 \times 10^6\ \mathrm{J\ m^{-3}\ °C^{-1}}$ and $\Delta z = 0.5$ m.
2. The Bowen ratio for five sites is: 0.5, 1.0, 6.0, 1.5, 0.2. Which site is the driest? Which site is the wettest?
3. Annual precipitation is 800 mm and annual net radiation is $70\ \mathrm{W\ m^{-2}}$. Which is more likely to limit annual evaporation: energy or water?
4. Use (13.5) to calculate annual evaporation for a site with $P = 1200$ mm and $R_n = 60\ \mathrm{W\ m^{-2}}$ and a second site with $P = 800$ mm and $R_n = 100\ \mathrm{W\ m^{-2}}$. Which site has greater runoff?

5. At a particular site, daily average $R_n = 120\ \mathrm{W\,m^{-2}}$ and $P = 8\ \mathrm{mm\,day^{-1}}$. Which is more likely to limit evaporation: energy or water? Assume no inter-seasonal water storage.
6. In Fig. 13.7, latent heat flux at the tropical rainforest increases at a faster rate with respect to net radiation (slope = 0.70) than at the grassland (slope = 0.45). Why might this be?
7. Use the Penman–Monteith equation to calculate latent heat flux for the following conditions: $R_n - G = 400\ \mathrm{W\,m^{-2}}$, $e_*[T_a] = 3169$ Pa and $s = 189\ \mathrm{Pa\,°C^{-1}}$ (values for $T_a = 25$ °C), $r_H = 25\ \mathrm{s\,m^{-1}}$ and $r_W = 50\ \mathrm{s\,m^{-1}}$. (a) Relative humidity is 75%. (b) Relative humidity is 50%. Use $\rho = 1.15\ \mathrm{kg\,m^{-3}}$, $C_p = 1005\ \mathrm{J\,kg^{-1}\,°C^{-1}}$, and $\gamma = 66.5\ \mathrm{Pa\,°C^{-1}}$.
8. Calculate surface temperature for 7(a) and 7(b). Why does surface temperature vary with relative humidity?
9. From (13.20), what is the sensitivity of surface temperature to a $1\ \mathrm{W\,m^{-2}}$ change in $R_n - G$? How do r_H and r_W affect this sensitivity?

13.10 References

Avissar, R. and Y. Mahrer, 1982. Verification study of a numerical greenhouse microclimate model. *Transactions of the American Society of Agricultural Engineers*, **25**, 1711–20.

Baldocchi, D. D., C. A. Vogel, and B. Hall, 1997. Seasonal variation of energy and water vapor exchange rates above and below a boreal jack pine forest canopy. *Journal of Geophysical Research*, **102D**, 28 939–51.

Betts, A. K. and J. H. Ball, 1998. FIFE surface climate and site-average dataset 1987–89. *Journal of the Atmospheric Sciences*, **55**, 1091–108.

Blanken, P. D., T. A. Black, P. C. Yang, *et al.*, 1997. Energy balance and canopy conductance of a boreal aspen forest: partitioning overstory and understory components. *Journal of Geophysical Research*, **102D**, 28 915–27.

Bonan, G. B., K. J. Davis, D. Baldocchi, D. Fitzjarrald, and H. Neumann, 1997. Comparison of the NCAR LSM1 land surface model with BOREAS aspen and jack pine tower fluxes. *Journal of Geophysical Research*, **102D**, 29 065–75.

Budyko, M. I., 1974. *Climate and Life*. Academic Press, 508 pp.

1986. *The Evolution of the Biosphere*. Reidel, 423 pp.

Campbell, G. S. and J. M. Norman, 1998. *An Introduction to Environmental Biophysics*, 2nd edn. Springer-Verlag, 286 pp.

Gash, J. H. C., C. A. Nobre, J. M. Roberts, and R. L. Victoria, 1996. An overview of ABRACOS. In *Amazonian Deforestation and Climate*, ed. J. H. C. Gash, C. A. Nobre, J. M. Roberts, and R. L. Victoria. Wiley, pp. 1–14.

Gates, D. M., 1980. *Biophysical Ecology*. Springer-Verlag, 611 pp.

Grace, J., 1983. *Plant–Atmosphere Relationships*. Chapman and Hall, 92 pp.

Grace, J., J. LLoyd, J. McIntyre, *et al.*, 1995. Fluxes of carbon dioxide and water vapour over an undisturbed tropical forest in south-west Amazonia. *Global Change Biology*, **1**, 1–12.

Grace, J., J. LLoyd, J. McIntyre, *et al.*, 1996. Carbon dioxide flux over Amazonian rain forest in Rondônia. In *Amazonian Deforestation and Climate*, ed. J. H. C. Gash, C. A. Nobre, J. M. Roberts, and R. L. Victoria. Wiley, pp. 307–18.

Koster, R. D., T. Oki, and M. J. Suarez, 1999. The offline validation of land surface models: assessing success at the annual timescale. *Journal of the Meteorological Society of Japan*, **77**, 257–363.

Mahrer, Y., R. Avissar, O. Naot, and J. Katan, 1987. Intensified soil solarization with closed greenhouses: numerical and experimental studies. *Agricultural and Forest Meteorology*, **41**, 325–34.

Milly, P. C. D., 1994. Climate, soil water storage, and the average annual water balance. *Water Resources Research*, **30**, 2143–56.

Monteith, J. L., 1965. Evaporation and environment. In *The State and Movement of Water in Living Organisms (19th Symposia of the Society for Experimental Biology)*, ed. G. E. Fogg. Academic Press, pp. 205–34.

1981. Evaporation and surface temperature. *Quarterly Journal of the Royal Meteorological Society*, **107**, 1–27.

Monteith, J. L. and M. H. Unsworth, 1990. *Principles of Environmental Physics*, 2nd edn. Edward Arnold, 291 pp.

Moore, K. E., D. R. Fitzjarrald, R. K. Sakai, and J. M. Freedman, 2000. Growing season water balance at a boreal jack pine forest. *Water Resources Research*, **36**, 483–94.

Oke, T. R., 1987. *Boundary Layer Climates*, 2nd edn. Routledge, 435 pp.

Penman, H. L., 1948. Natural evaporation from open water, bare soil and grass. *Proceedings of the Royal Society of London*, **193A**, 120–45.

Rosenberg, N. J., B. L. Blad, and S. B. Verma, 1983. *Microclimate: the Biological Environment*, 2nd edn. Wiley, 495 pp.

Sellers, W. D., 1965. *Physical Climatology*. University of Chicago Press, 272 pp.

Stanhill, G., 1965. Observations on the reduction of soil temperature. *Agricultural Meteorology*, **2**, 197–203.

Unland, H. E., P. R. Houser, W. J. Shuttleworth, and Z.-L. Yang, 1996. Surface flux measurement and modeling at a semi-arid Sonoran Desert site. *Agricultural and Forest Meteorology*, **82**, 119–53.